SCIENCE CHINA
Technological Sciences

•Article•

December 2023 Vol.66 No.12: 3522–3533
https://doi.org/10.1007/s11431-023-2475-3

Mechanical properties and shape memory behavior of 4D printed functionally graded cellular structures

ZENG ChengJun[1], LIU LiWu[1], ZHAO Wei[1], LIU ZhengXian[2], XIN XiaoZhou[1], LIU YanJu[1*] & LENG JinSong[2]

[1] *Department of Astronautical Science and Mechanics, Harbin Institute of Technology, Harbin 150001, China;*
[2] *Center for Composite Materials and Structures, Harbin Institute of Technology, Harbin 150080, China*

Received April 29, 2023; accepted July 24, 2023; published online November 1, 2023

The properties of functionally graded (FG) cellular structures vary spatially, and the varying properties can meet the requirements of different working environments. In this study, we fabricated FG cellular structures with shape memory effect by 4D printing and evaluated the compressive performance and shape memory behavior of these structures with temperature through experimental analysis and finite element simulations. The results show that the maximum energy absorption gradually decreases but the compressive modulus gradually increases with increasing gradient parameters. Moreover, the finite element simulations also show that the compressive deformation mode of the structure shifts from uniform to non-uniform deformation with increasing gradient parameters. The compressive modulus and compressive strength of 4D printed FG structures decrease with increasing temperature due to the influence of the shape memory polymer, and they exhibit outstanding shape recovery capability under high-temperature stimulus. The proposed 4D printed FG structures with such responsiveness to stimulus shed light on the design of intelligent energy-absorbing devices that meet specific functional requirements.

functionally graded structures, 4D printing, shape memory polymers, energy absorption, cellular structures

Citation: Zeng C J, Liu L W, Zhao W, et al. Mechanical properties and shape memory behavior of 4D printed functionally graded cellular structures. Sci China Tech Sci, 2023, 66: 3522–3533, https://doi.org/10.1007/s11431-023-2475-3

1 Introduction

Inspired by natural materials, cellular structures are lattices composed of interconnected or individually closed pores, which have many characteristics that conventional materials do not possess, such as outstanding load-bearing capacities, high energy absorption characteristics, and thermal/sound insulation properties [1–4]. Guided by practical application, the material can be fully utilized by designing the unit cell of cellular structure, thereby reducing production costs and obtaining lightweight products. For example, tensile-dominated cells such as octagonal trusses and Kagome lattices enable high stiffness and strength of cellular structures [5]. Bending-dominated cells, such as hexagonal honeycombs and body-centered cubic lattices, are potentially advantageous in energy absorption applications due to their long stress plateaus in the compression mode [6]. In addition, some trapezoidal or sinusoidal corrugated unit cells have extremely anisotropic mechanical behavior and thus exhibit great potential in engineering applications such as morphing wings. These cells are flexible in the corrugated direction and can change shape, but their high stiffness-to-mass ratio in the transverse direction perpendicular to the corrugated direction offers them the ability to withstand extreme mechanical loads [7].

Recently, some cellular structures with functionally graded (FG) characteristics have attracted the attention of researchers, which makes the material or geometry change

*Corresponding author (email: yj_liu@hit.edu.cn)

continuously in a certain direction [8–11]. After the rational design, the response pattern of FG cellular structures can vary with the loading process or the working environment, and then meet the requirements of specific engineering applications. Currently, two main types of FG cellular structures have been proposed, namely size-graded cellular structures and material-graded cellular structures. Size-graded cellular structures achieve gradient changes in structural features by changing the cell configuration or scaling the cell size [8]. However, the production of these FG cellular structures with complex non-uniform features is challenging due to the limitations of conventional processes such as electrical machining and CNC cutting.

Recent advances in additive manufacturing (also known as 3D printing) have enabled the fabrication of cellular structures with complex microstructures or non-uniform gradient features [12–14]. For example, Kuang et al. [15] manufactured FG lattice structures with tunable buckling and well-controlled deformation sequence by the gray-scale digital light processing (gDLP) technique. Montgomery et al. [16] recently fabricated FG foam by this method, which possesses improved impact mitigation capabilities compared to homogeneous foam. Al-Saedi et al. [17] prepared 3D metal lattice structures with FG features by selective laser melting (SLM) process and investigated the mechanical performance and energy absorption capabilities of FG lattice structures by compression experiments and finite element analysis. Sinusoidal corrugated structures are widely used as mechanical protection components in aerospace, transportation, and marine engineering because of their smooth curve configurations that can greatly weaken stress concentrations. Recently, Zhang et al. [18] reported 3D printed multi-layered sinusoidal corrugated sandwich structures with FG characteristics and preliminarily revealed the effect of gradient design on compressive performance and energy absorption capabilities of sandwich structures. Despite these advances, the production of cellular structures with active deformability and tunable mechanical properties by 3D printing remains a challenge.

4D printing, combining stimulus-responsive materials and 3D printing processes, offers an unprecedented way to personalize actively deformable and mechanically tunable cellular structures [19–21]. 4D printed objects can change their shape or properties over time in response to various external stimuli [22–24]. Recently, Bodaghi et al. [25,26] produced dual-material auxetic meta-sandwiches and re-entrant auxetic mechanical metamaterials with reversible energy absorption capability by fused filament fabrication (FFF) 4D printing technique. Liu et al. [27] proposed 4D printed metamaterials with zero Poisson's ratio characteristics, which exhibit vibration isolation and can convert mechanical properties by sensing temperature changes. Wang et al. [28] fabricated multi-patterned composite metamaterials with adjustable Poisson's ratio and band gap by 4D printing. Zeng et al. [29–31] manufactured a variety of 4D printed composite lightweight structures with desirable mechanical characteristics and active deformation capabilities based on shape memory polymers (SMPs). As can be seen from the above progress, the current research on FG cellular structures is limited to the development of gradient strategies and the verification of mechanical properties such as compressive properties, and no systematic studies of 4D printed FG cellular structures with active deformation capability have been published. Moreover, the current studies have not yet paid attention to the temperature-dependent mechanical behavior of FG cellular structures.

In view of the above challenges, this study proposes 4D printed multi-layer sinusoidal corrugated cellular structures with power-type gradient characteristics. Thanks to the incorporation of SMP, 4D printed FG cellular structures exhibit exceptional temperature-dependent mechanical properties and shape memory behavior. The effects of the gradient parameters on the temperature-dependent compressive modulus, compressive strength and energy absorption capacity of 4D printed FG cellular structures are investigated by compression experiments, and the deformation patterns of the FG cellular structures are announced in conjunction with finite element simulations. In addition, we demonstrate the thermally-induced shape recovery process of 4D printed FG cellular structures, providing a competitive solution for the design of stimulus-responsive intelligent gradient cellular structures.

2 Materials and methods

2.1 Structural design

Nature-inspired sinusoidal corrugated cellular structures possess excellent energy absorption capacities and their smooth curvilinear configurations can greatly weaken stress concentrations and enhance the load-bearing capacity of structures compared to conventional rectangular, triangular or trapezoidal corrugated cellular structures with inflection points. To describe the periodic sinusoidal corrugated cellular structure, a series of geometric parameters are defined as wall thickness t, period of the sinusoidal wave T and height of the n-th layer h_n. Therefore, the envelope of sinusoidal corrugated cellular structures can be represented by the following equation [32]:

$$y = \frac{h_n}{2}\sin\left(\frac{2\pi}{T}x\right). \tag{1}$$

Compared with single-layer corrugated structures, multi-layer corrugated structures further enhance crashworthiness thanks to their progressive damage process. As shown in Figure 1(a), by adjusting the height h_n of every single layer, a

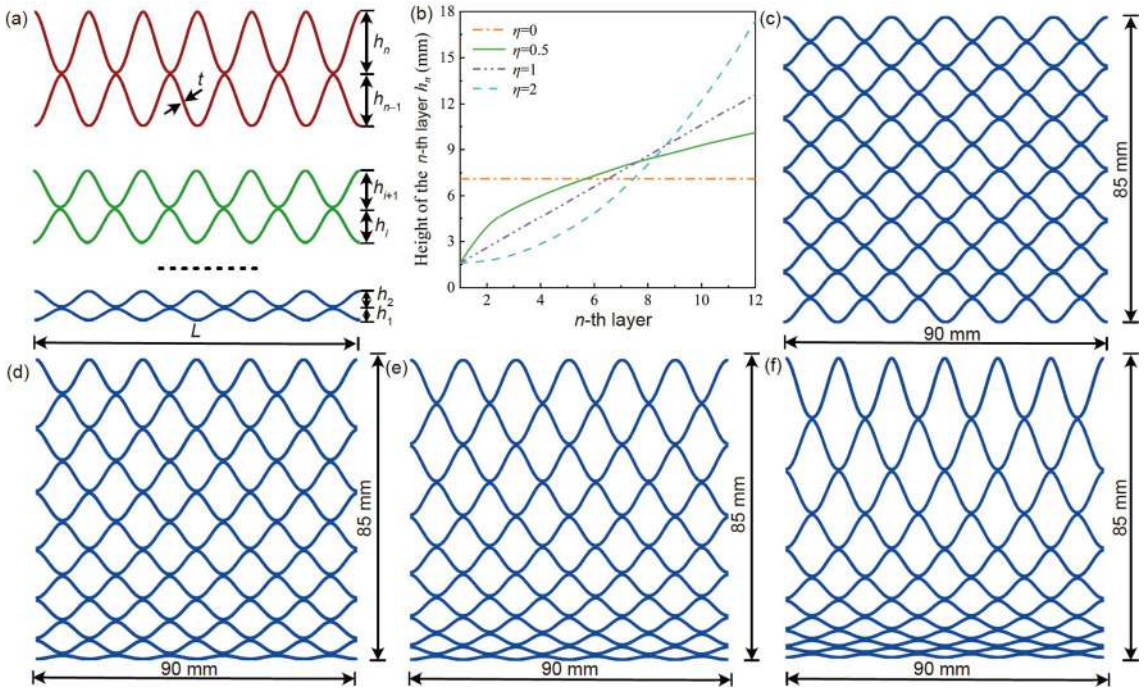

Figure 1 (Color online) Design of multi-layer FG corrugated cellular structures. (a) Illustration of size-graded characteristics of multi-layer corrugated cellular structures; (b) evolution curves of the layer height h_n for different gradient parameters η; 2D plan view of FG cellular structures for gradient parameters (c) η = 0, (d) η = 0.5, (e) η = 1 and (f) η = 2.

multi-layer FG corrugated structure with size-graded characteristics can be obtained. In this work, a power-type function is proposed to describe the size-graded characteristics of the multi-layer FG corrugated structure:

$$h_n = \frac{H - Nh_1}{\sum_{i=1}^{N}(i-1)^{\eta}}(n-1)^{\eta} + h_1, \tag{2}$$

where N is the number of layers of multi-layer FG corrugated cellular structures; h_1 is the height of the first layer; H is the total height of cellular structures and $H = \sum_{n=1}^{N} h_n$; η is the power-type gradient parameter, η = 0 means the height of every single layer is the same.

In this work, the above structural parameters are determined as the wall thickness t = 0.9 mm, the number of layers N = 12 and total height H = 85 mm. The gradient parameter η is used as a key parameter to determine the gradient features of multi-layer corrugated cellular structures, which affects the mechanical performance and energy absorption of structures. According to the mathematical characteristics of the power-type function, four typical gradient parameters η are selected in this study to investigate the mechanical response of multi-layer FG cellular structures, i.e., η = 0, 0.5, 1 and 2. Figure 1(b) shows the evolution trend of the layer height h_n for different gradient parameters η, from which it can be observed that the layer height h_n increases linearly with the number of layers n for η = 1, which corresponds to the linear FG structure. When η = 0.5 or η = 2, the evolution curve of h_n is convex or concave, respectively. All structures have a width of 90 mm and an out-of-plane thickness of 30 mm (Figure 1(c)–(f)).

2.2 Sample fabrication

Combining 3D printing and stimulus-responsive materials, 4D printing enables the integrated creation of active devices that can change their shape and/or function on demand over time. The four FG structures presented in Section 2.1 were fabricated by 4D printing. The equipment used for 4D printing was an FFF 3D printer (Anycubic Mega-S). The printing consumable was a polylactic acid (PLA)-based SMP filament, which possessed excellent shape memory properties [33]. A moderate printing speed of 30 mm/s was adopted to obtain a trade-off between printing efficiency and printing accuracy. The melt temperature of the SMP filament was about 170°C, so a slightly higher nozzle temperature of 210°C was used. The nozzle diameter and platform temperature were 0.4 mm and 60°C, respectively. Figure 2 presents samples of FG structures prepared by 4D printing with various gradient parameters η. All samples have an envelope size of 90 mm × 85 mm × 30 mm. Furthermore, the relative density of all samples ranges between 15.3% and 16.2%.

2.3 Experimental procedure

To evaluate the influence of gradient parameter η on the thermomechanical properties of 4D printed FG structures,

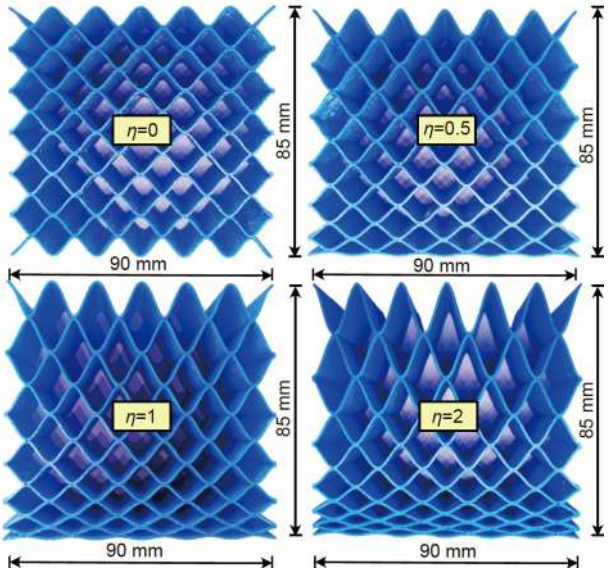

Figure 2 (Color online) Samples of FG structures with different gradient parameters η fabricated by 4D printing.

quasi-static compression tests and shape memory cycling tests at different temperatures were carried out. The quasi-static compression tests were conducted by a Zwick/Roell machine with an environmental chamber, and four isothermal conditions were set, namely 25°C, 45°C, 55°C and 65°C. According to standard ASTMD1621, the loading rate during compression was selected as 4 mm/min, and the compression continued until the densification stage. For each case, three identical samples were tested to ensure the reproducibility of experimental results. A digital camera was applied to capture the compression deformation pattern of samples.

Since the raw material is shape memory polymer, 4D printed FG structures exhibit the shape memory effect. 4D printed FG structures were subjected to shape memory cycling tests to characterize this shape memory effect, which was conducted in compression mode. The shape memory cycling test was carried out in four steps. Firstly, the sample was compressed by 20 mm with a rate of 5 mm/min at 70°C, and it was ensured that the sample was held in an isothermal environment at 70°C for more than 15 min before loading. Secondly, keeping the displacement constant, the sample was cooled from 70°C to 25°C. Then, maintaining the temperature at 25°C and unloading the load, the temporary shape of the sample was fixed. Finally, the sample was heated from 25°C to 70°C while keeping the load at zero, during which the sample gradually recovered from the temporary shape to the original shape. During the shape recovery process, the evolution curve of displacement over time and the deformation image of the sample were recorded.

In order to perform finite element simulations for the compression process of 4D printed FG structures, it is necessary to characterize the material properties of the raw material. SMP-based dogbone tensile coupons with a thickness of 2 mm were prepared by 3D printing according to ASTM standard D638, and the other dimensions of the coupons are shown in Figure 3(a). Since the printing direction of ±45° can provide an approximation for assessing material properties of 3D printed materials, all tensile coupons were fabricated in the direction of ±45° relative to the loading axis [34]. Quasi-static tensile tests of coupons were carried out at four temperatures, i.e., 25°C, 45°C, 55°C and 65°C. The gauge length and loading rate were 40 mm and 2 mm/min, respectively. Figure 3(b) presents the tensile stress-strain curves of 3D printed materials, from which it is observed that the mechanical properties vary significantly at different temperatures, which is attributed to the variable stiffness effect of SMP. PLA-based SMP is a thermotropic variable stiffness material whose Young's modulus decreases significantly with the increasing temperature near the glass transition temperature [33].

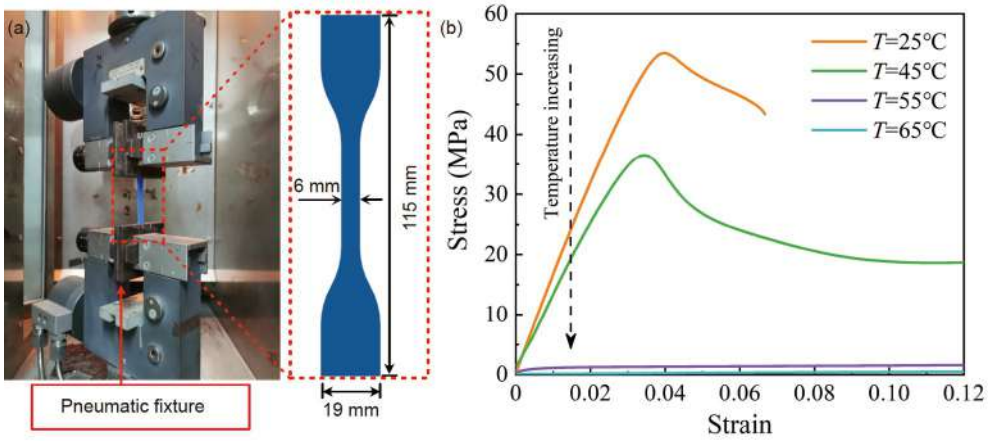

Figure 3 (Color online) Quasi-static tensile testing of 3D printed SMP coupons. (a) Coupon geometry and test equipment; (b) true stress-strain curves at various temperatures.

2.4 Numerical simulation

Finite element simulations were performed with the commercial finite element software ABAQUS/EXPLICIT 2020 to reveal the compressive deformation mechanism of 4D printed FG structures. 3D finite element models of one uniform structure ($\eta = 0$) and three FG structures ($\eta = 0.5$, 1 and 2) were established according to the designed geometry. An eight-node hexahedral linear element with reduced integration (C3D8R) was used in all finite element models to obtain the trade-off computational accuracy and efficiency. Rigid plates were created at the top and bottom of the structure to incorporate experimental-like boundary conditions, where the top rigid plate moved uniformly in the z-direction to simulate the compressive loading process, while the bottom plate was constrained in all degrees of freedom. Generic contact was used to simulate the contact interaction among parts of the model and a "hard" contact with frictional tangential behavior was defined for the whole model. The mesh convergence analysis was performed on the models to obtain the appropriate mesh size, and each model was divided into approximately 240000 elements. Since the PLA-based SMP exhibits the post-yield effect, the material properties of the PLA-based SMP were simulated in ABAQUS using an isotropic plasticity model. The material parameters to be input include density, Young's modulus, Poisson's ratio and plastic parameters, where the density and Poisson's ratio are taken as 1250 kg/m^3 and 0.4, respectively. The Young's modulus and plastic parameters at different temperatures can be determined from the true stress-strain curves given in Figure 3(b), and the obtained parameters are listed in Table 1. It should be noted that the PLA-based SMP exhibits fully elastic behavior at 65°C, so no plastic parameters are input.

3 Results and discussion

3.1 Compressive mechanical properties

The equivalent stress-strain response of 4D printed FG structures can be determined by processing the load-displacement data obtained during compression. Figure 4 presents a comparison of experimental compressive stress-strain curves for 4D printed FG structures at room temperature (25°C) with simulated ones. From experimental results in Figure 4(a), it can be found that the uniform structure ($\eta = 0$) undergoes initial elastic deformation up to a strain level of 0.08. With further increase in compressive strain, the yielding and plastic collapse of webs occur in the structure, which is manifested macroscopically as the plastic yield point and initial peak in the stress-strain curve. After the initial yielding of the structure, the stress-strain curve enters the plateau evolution phase, in which the load-bearing capacity of the structure remains generally stable with the increase of the compressive strain. When the compressive strain reaches 0.8, the stress increases steeply with the increase of strain, which indicates that the stress-strain curve enters the densification phase. The structure is compacted in the densification phase, which results in an enhanced load-bearing capacity of the structure. Comparing the experimental measurement and finite element simulation in Figure 4(a), it can be found that the stress-strain curve obtained from the simulation has a delay in the initial yielding compared with that obtained from the experiment, but the evolution trend of the stress plateau obtained from the simulation and the experiment is the same.

The gradient design of FG structures makes their compressive response more complicated compared with the uniform structure. The equivalent stress-strain curves of 4D printed FG structures for gradient parameters $\eta = 0.5$, $\eta = 1$ and $\eta = 2$ are given in Figure 4(b)–(d), respectively. An obvious observation is that the gradient design shortens the plateau phase in the stress-strain curve and reduces the initial load peak, with a distinct second or even third stress peak in the stress-strain curve. In fact, the gradient design endows each layer in the multi-layer structure with a different load-bearing capacity, where the layers with small layer heights exhibit degraded mechanical properties, which leads to stepwise fluctuations of the stress in the structure during layer-by-layer failure [18]. Conversely, all single layers in the uniform multi-layer structure possess the same load-bearing capacity, so their progressive failure does not cause

Table 1 Young's modulus and true plastic stress/strain of the raw material at various temperatures

25°C			45°C			55°C			65°C
Modulus (MPa)	Yield stress (MPa)	Plastic strain	Modulus (MPa)	Yield stress (MPa)	Plastic strain	Modulus (MPa)	Yield stress (MPa)	Plastic strain	Modulus (MPa)
	32.1	0		19.62	0		1.12	0	
	38.17	0.004		24.2	0.004		1.19	0.004	
	43.93	0.009		29.52	0.009		1.23	0.009	
1600	49.01	0.013	1249	33.17	0.013	93	1.25	0.013	3.5
	53.18	0.021		36.19	0.021		1.28	0.021	
	48.96	0.031		28.62	0.031		1.31	0.031	
	43.36	0.047		23.63	0.047		1.36	0.047	

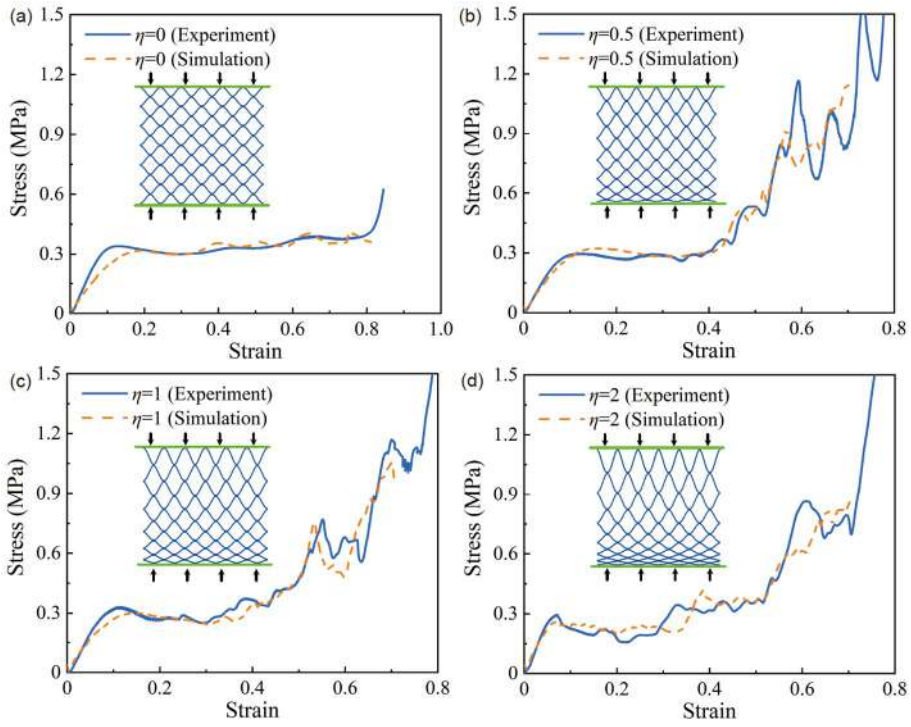

Figure 4 (Color online) Experiments and simulations of 4D printed FG structures with gradient parameters. (a) $\eta = 0$, (b) $\eta = 0.5$, (c) $\eta = 1$, and (d) $\eta = 2$ for compressive stress-strain response at room temperature.

large perturbations in the stress.

The gradient parameter η is a key parameter to measure the variability of each single-layer corrugated structure in 4D printed FG structure. In general, a larger value of η represents a more significant difference in load-bearing capacity among individual single-layer corrugated structures, which can cause more pronounced stress fluctuations. By comparing the experimental results in Figure 4(b)–(d), it is found that the stress-strain curve fluctuates more significantly during the plateau evolution phase as η increases, which is consistent with the above analysis. In addition to experiments, finite element simulations are also able to effectively predict the compressive stress-strain response of 4D printed FG structures. The compressive stress-strain curves obtained from experiments are in good agreement with those from finite element simulations (Figure 4).

SMP is a thermoplastic material with temperature-dependent mechanical properties. Therefore, we investigate the temperature-dependent compressive response of 4D printed FG structures. The equivalent stress-strain curves for structures with different gradient parameters at 45°C and 55°C are plotted in Figure 5. It should be noted that the stress response is much lower than that at 55°C when the temperature is 65°C. Therefore, the stress-strain curve at 65°C is not presented here. From Figures 4 and 5, it can be found that the stress at the same strain gradually decreases as the temperature increases. The evolution trend of stress-strain curves at 45°C is generally consistent with that at 25°C, indicating that 4D printed FG structures still maintain excellent load-bearing capacity at 45°C. However, as the temperature rises further to 55°C, the stress response is greatly weakened, which is attributed to the sharp decrease in the elastic modulus of SMP near the glass transition temperature. In addition, SMP exhibits obvious plastic yielding and strain softening phenomena at 45°C, but plasticity diminishes and the strain softening phenomena disappear as the temperature is raised to 55°C. Therefore, stress-strain curves of 4D printed FG structures become smooth at 55°C.

Figure 6(a) and (b) depict the experimentally obtained evolution curves of compressive modulus and compressive strength over temperature for 4D printed FG structures, respectively. The compressive modulus is calculated from the linear segment of the stress-strain curve. When the gradient parameter η is the same, the evolution curve of compressive modulus over temperature shows an S-shaped trend. The temperature interval with the fastest drop in compressive modulus is the interval from 45°C to 55°C. This finding is consistent with the previous analysis. By observing Figure 6(a), it is found that the compressive modulus increases with the gradient parameter η at 25°C and 45°C, and the structure with $\eta = 2$ possesses the largest compressive modulus. When the temperature is 55°C or 65°C, the gradient parameter causes less effect on the compressive modulus. The compressive strength denotes the initial ultimate stress in the stress-strain curve. When the gradient parameter is the same, the evolution trend of compressive strength over

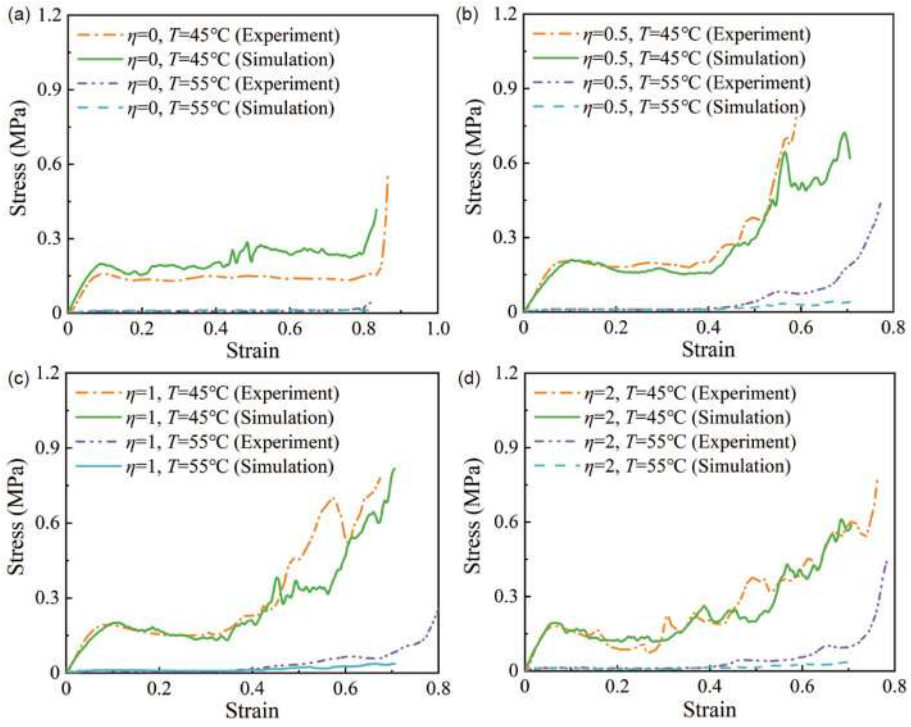

Figure 5 (Color online) Experiments and simulations of 4D printed FG structures with gradient parameters. (a) $\eta = 0$, (b) $\eta = 0.5$, (c) $\eta = 1$, and (d) $\eta = 2$ for compressive stress-strain response at high temperature.

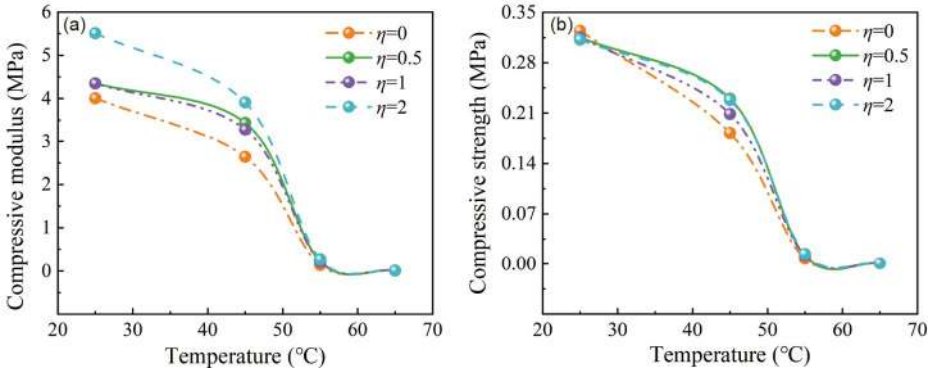

Figure 6 (Color online) (a) Compressive modulus and (b) compressive strength of 4D printed FG structures at different temperatures.

temperature is similar to that of compressive modulus (Figure 6(b)). It should be noted that the gradient parameter poses little effect on the compressive strength at 25°C.

3.2 Energy absorption capacities

The maximum energy absorption per unit volume of the cellular structure is determined by the area under the stress-strain curve prior to the densification phase [35]:

$$W = \int_0^{\varepsilon_d} \sigma(\varepsilon) \mathrm{d}\varepsilon, \tag{3}$$

where the densification strain ε_d denotes the strain when maximum energy absorption efficiency is achieved. As can be seen in Figure 4, the densification strain is about 0.75 for the uniform structure ($\eta = 0$) at room temperature, while the densification strain is about 0.5 for FG structures ($\eta = 0.5$, 1 or 2).

Figure 7 summarizes the experimental measurements and finite element simulations of the maximum energy absorption per unit volume at room temperature for 4D printed FG structures with different gradient parameters. The uniform structure has significantly higher maximum energy absorption compared with FG structures, which is attributed to its long stress plateau phase. In fact, the gradient design enhances the inhomogeneity of the structure, which imparts a smaller densification strain on the structure. Although the gradient design weakens the maximum energy absorption of the cellular structure, it effectively reduces the reaction force

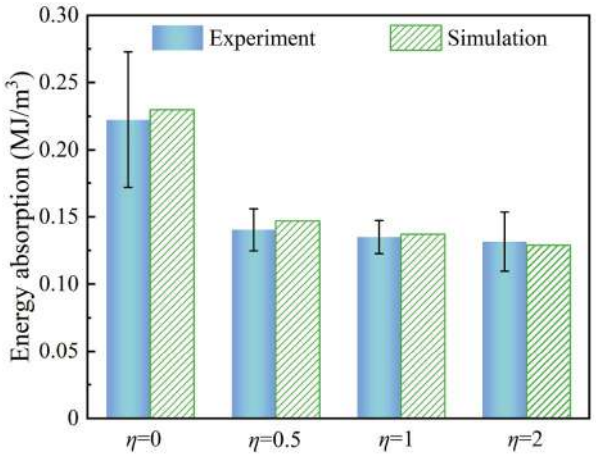

Figure 7 (Color online) Experimental measurements and finite element simulations for the maximum energy absorption per unit volume of 4D printed FG structures with different gradient parameters η at room temperature.

during loading, which is more suitable for sacrificial materials. The gradient parameter η affects the maximum energy absorption of 4D printed FG structures. When the gradient parameter varies from $\eta = 0$ to $\eta = 0.5$, the maximum energy absorption obtained experimentally is reduced by 39.3%, which is significantly greater than that when the gradient parameter varies from $\eta = 0.5$ to $\eta = 2$. This phenomenon indicates that the gradient parameter of 0.5 has significantly affected the energy absorption of the structure, and further increase of the gradient parameter will not cause a more substantial change in the maximum energy absorption. In addition, Figure 7 presents a comparison of the experimental and simulated maximum energy absorption. The results demonstrate that the maximum energy absorption obtained by simulations is in general agreement with the average value obtained by experiments.

Energy absorption diagrams provide a way to characterize the energy absorption capacity of cellular structures, which allows the design of optimal geometrical configurations for specific applications [36]. The energy absorption diagram establishes the relationship between the two most important parameters required for energy absorption applications, i.e., energy absorption per unit volume and the maximum stress generated on the protected object. Figure 8(a) plots the experimental and simulated energy absorption for the uniform structure ($\eta = 0$) and linear graded structure ($\eta = 1$). Each energy curve starts with a slow rise, which corresponds to the initial elastic section of the stress-strain curve. When the plateau phase is reached, a sudden increase occurs in the energy curve. As the structure is further compacted, the slope of the energy curve gradually decreases. The shoulder in the energy curve corresponds to the onset of densification, and maximum stresses at the onset of densification are very close for the uniform and linear graded structures, but the uniform structure possesses higher energy absorption (Figure 8(a)). For each structure, the simulated energy profiles approximately coincide with the experimental ones. Figure 8(b) presents the experimental energy profiles for 4D printed FG structures with various gradient parameters η, from which it can be found that the gradient parameter poses little effect on energy profiles.

3.3 Compressive deformation modes

The analysis of compressive deformation modes facilitates the evaluation of mechanical properties and failure behavior of 4D printed FG structures. Figure 9(a) presents a comparison between experimental and simulated compressive deformation processes for a uniform multi-layer cellular structure ($\eta = 0$). At low compressive strains, the structure exhibits uniform deformation. After the compressive strain reaches 0.42, lattices yield and collapse on both diagonals of the structure, leading to a pronounced double shear band. The shear failure mechanism announces the sensitivity of the structure to external boundary conditions and unit cell location. With a further increase in compressive strain, the failure of the structure gradually extends from the collapse of

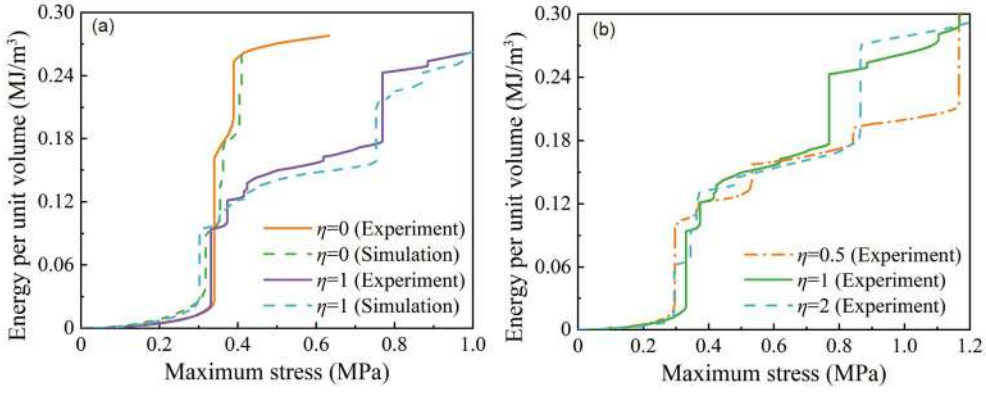

Figure 8 (Color online) Energy absorption diagrams of 4D printed FG structures. (a) Experimental and simulated energy absorption diagrams for uniform structure ($\eta = 0$) and linear graded structure ($\eta = 1$). (b) Experimental energy absorption diagrams of FG structures with different gradient parameters.

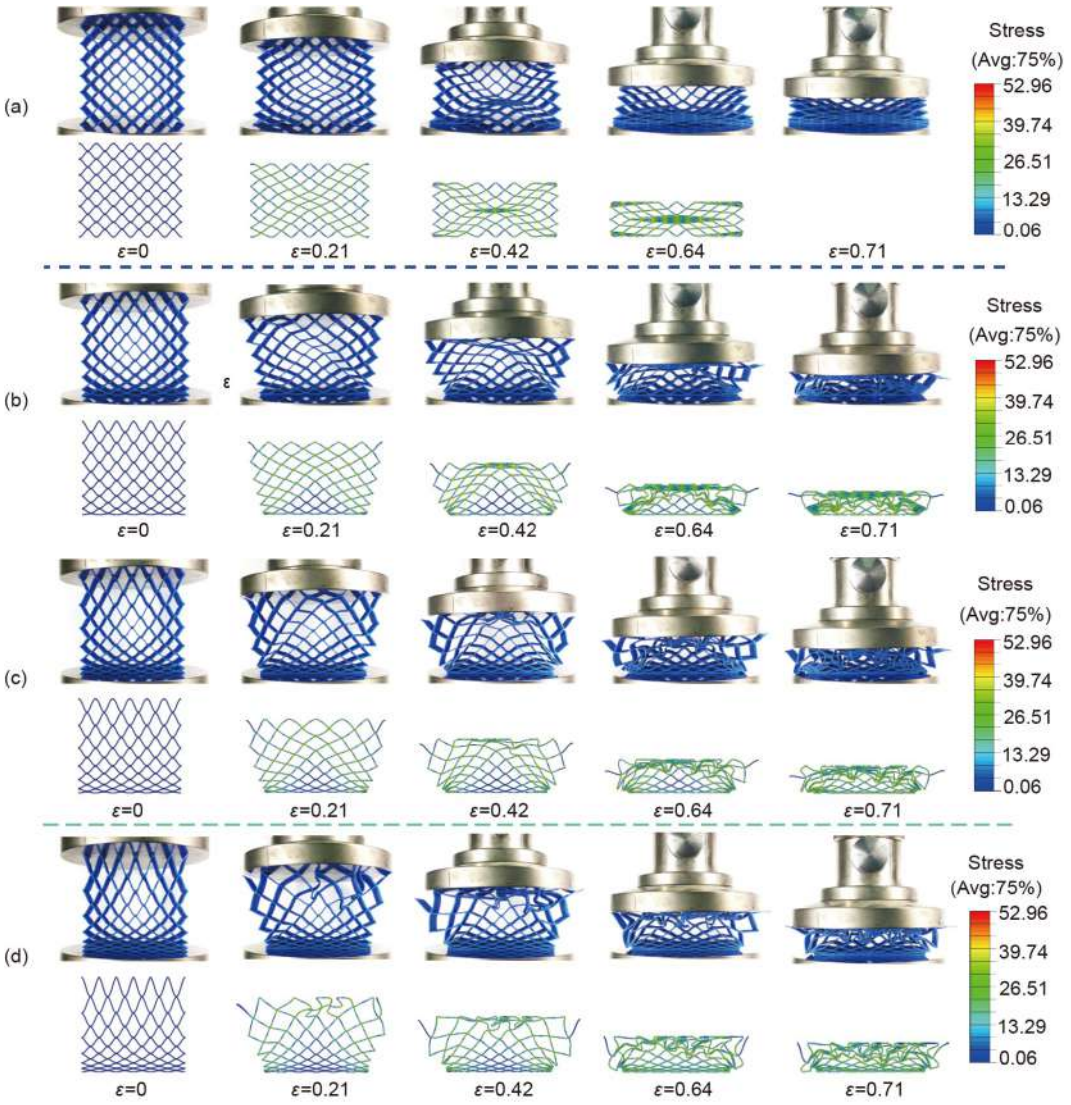

Figure 9 (Color online) Experimental and simulated deformation patterns of 4D printed FG structure with gradient parameters (a) $\eta = 0$, (b) $\eta = 0.5$, (c) $\eta = 1$, and (d) $\eta = 2$.

lattices on the diagonals to layer-by-layer collapse, which leads to structural densification. In addition, an important observation is that lattices near the middle of the upper and lower boundaries remain uncollapsed throughout the compression process, indicating its potential as a protective structure for precision devices.

Unlike the deformation mechanism of the uniform multi-layer cellular structure, FG structures undergo uneven deformation during the compression process, and the gradient parameter η affects the deformation pattern of structures. Experiments and simulations of the compressive deformation process for 4D printed FG structures with $\eta = 0.5$, $\eta = 1$ and $\eta = 2$ are given in Figure 9(b)–(d), respectively, from which the differences in the deformation modes of several FG structures can be noticed. At lower strain levels, the deformation of the FG structure occurs mainly in the diagonal region of the structure and the region with larger single-layer height, which is different from the double shear deformation mechanism of the uniform structure. Lattices on both sides of structures expand to the outside during compression because transverse degrees of freedom are not restricted. The gradient design allows the single-layer height of the multi-layer structure to vary gradually in the compression direction, which leads to different amounts of outward deformation of lattices on both sides of the structure. A general observation is that the thicker the single-layer cellular structure is in the compression direction, the more prone it is to deform outward.

The gradient design also exerts an influence on the deformation pattern of lattices at the middle position of FG structures. As can be seen in Figure 9(b)–(d), lattices near the middle of the upper boundary collapse at a lower compressive strain, while lattices near the middle of the lower boundary remain uncollapsed during compression due to

higher stability. According to the graded distribution strategy of the single-layer height h_n shown in Figure 1(b), it can be found that the single-layer height increases gradually from the lower to the upper boundary of the structure. A large single-layer height corresponds to a long lattice strut, which is susceptible to buckling or yielding failure.

3.4 Shape memory behavior

The shape memory properties of 4D printed FG cellular structures were characterized according to the procedure described in Section 2.3 for shape memory cycling tests. Figure 10(a) presents displacement-time curves in shape memory cycling tests. During the loading phase, all samples were compressed by 20 mm at 70°C with the same loading rate, so their displacement-time curves overlapped at that phase. During the cooling phase, the temperature was uniformly lowered from 70°C to 25°C, so the displacement remained at 20 mm in this phase. Unloading was carried out after the cooling phase, and the displacement did not change during the unloading process, indicating that the shape fixity ratio of 4D printed FG cellular structure was close to 100%. After unloading, the temperature was raised from 25°C to 70°C, during which the shape memory effect of the material was triggered. The displacement-time curve of 4D printed FG cellular structure during the shape recovery process shows an S-shape, which shifts to the right on the time axis as the gradient parameter η increases (Figure 10(a)).

To evaluate the shape recovery performance of 4D printed FG cellular structures, the shape recovery ratio is expressed as shape recovery ratio = (maximum displacement – final displacement)/maximum displacement × 100%, where maximum displacement denotes the displacement after unloading and final displacement denotes the residual displacement after shape recovery [37]. Figure 10(b) presents the shape recovery ratio of 4D printed FG cellular structures with different gradient parameters η, from which it can be seen that the shape recovery ratio gradually decreases as η increases.

In general, a large gradient parameter η will lead to irreversible plastic deformation or failure of structures during compression, which reduces the shape recovery ratio. Figure 11(a) and (b) exhibit the deformation images of the uniform structure and FG structure with $\eta = 0.5$ during shape memory cycling, respectively. Images of samples at displacement $U = 0$, 5, 10 and 20 mm during loading are given, as well as the corresponding images during shape recovery. In agreement with the previous analysis, significant shape recovery phenomena are observed in Figure 11. It should be noted that samples possess residual displacement after shape recovery due to irreversible plastic deformation or local failure.

4 Conclusions

In this study, several FG corrugated cellular structures with different gradient parameters were designed and fabricated by 4D printing. Temperature-dependent finite element models were proposed to predict compressive responses and energy absorption characteristics of 4D printed FG structures and examined by corresponding compression tests. Finite element simulations agree well with the experimental measurements. When compressed at room temperature, the uniform structure (η = 0) has a longer stress plateau and therefore higher energy absorption compared with FG structures (η = 0.5, 1 or 2). The quantitative effect of the gradient parameter η on energy absorption should be considered in future studies. The compression response of 4D printed FG structure is temperature-dependent due to the thermotropic variable stiffness effect of SMP. Evolution curves of the compressive modulus and compressive strength with temperature show an S-shaped trend for the same gradient parameters. In addition, the gradient parameter η affects the compressive deformation pattern and failure mechanism of structures. Symmetric double shear bands

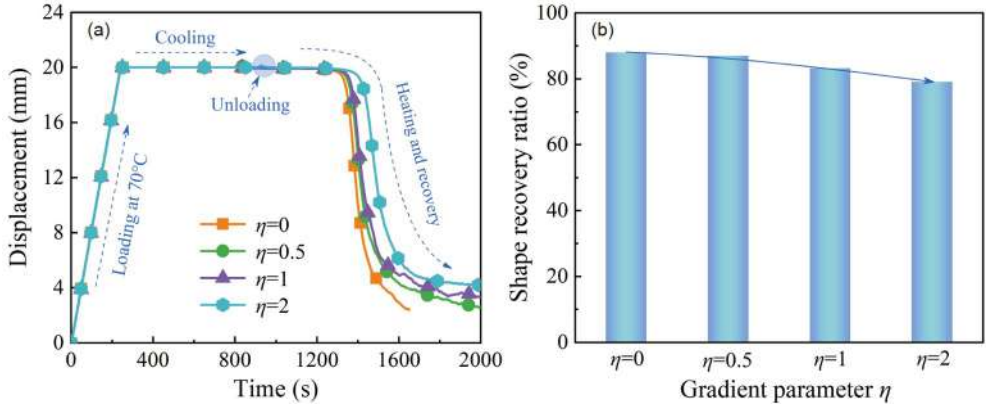

Figure 10 (Color online) (a) Displacement-time curves and (b) shape recovery ratio of 4D printed FG cellular structures in shape memory cycling tests.

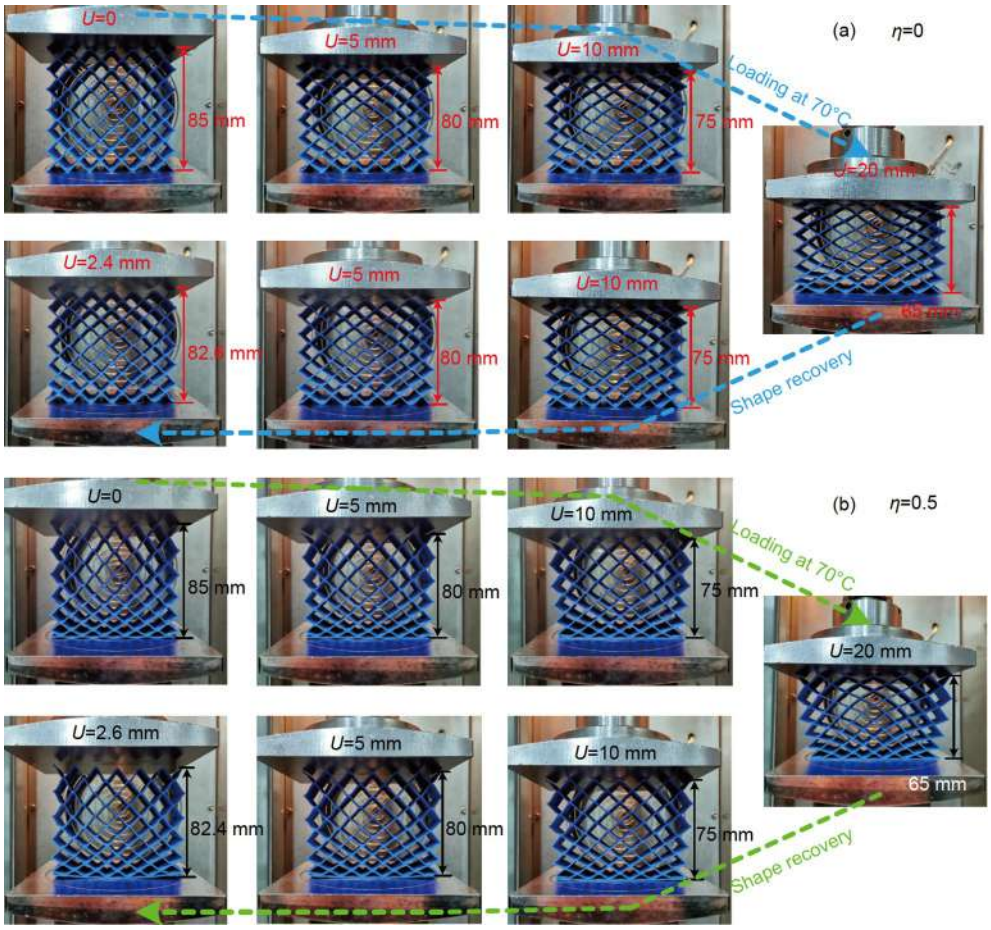

Figure 11 (Color online) Deformation images of structures with gradient parameters (a) $\eta = 0$ and (b) $\eta = 0.5$ during shape memory cycling.

appear on both diagonals of the uniform structure ($\eta = 0$) during compression, while the main deformation of FG structures ($\eta = 0.5$, 1 or 2) is concentrated in the region with a larger single-layer height. To characterize the shape memory performance of 4D printed FG structures, shape memory cycling tests were performed. The results indicate that the shape recovery ratio is above 80% for structures with different gradient parameters. The design strategy for FG structures presented in this work will provide great opportunities for the development of stimulus-responsive devices capable of meeting specific functional requirements, which can be widely used as attractive and highly intelligent energy-absorbing devices and other protective components.

This work was supported by the National Natural Science Foundation of China (Grant Nos. 12072094 and 12172106).

1 Zhang D J, Zhao Z Y, Du S F, et al. Dynamic response of ultralight all-metallic sandwich panel with 3D tube cellular core to shallow-buried explosives. Sci China Tech Sci, 2021, 64: 1371–1388
2 Dong J, Ye G, Wang Y, et al. Design, manufacture and crushing behaviors of buckling-inspired auxetic meta-lattice structures. Int J Smart Nano Mater, 2021, 12: 491–510
3 Al-Ketan O, Lee D-W, Abu Al-Rub R K. Mechanical properties of additively-manufactured sheet-based gyroidal stochastic cellular materials. Addit Manuf, 2021, 48: 102418
4 Huang Y, Chen E, Sun J, et al. Wave control of a flexible space tether based on elastic metamaterials. Int J Mech Sys Dyn, 2023, 3: 58–72
5 Zhang L, Feih S, Daynes S, et al. Energy absorption characteristics of metallic triply periodic minimal surface sheet structures under compressive loading. Addit Manuf, 2018, 23: 505–515
6 Yu X, Zhou J, Liang H, et al. Mechanical metamaterials associated with stiffness, rigidity and compressibility: A brief review. Prog Mater Sci, 2018, 94: 114–173
7 Mohammadi H, Ziaei-Rad S, Dayyani I. An equivalent model for trapezoidal corrugated cores based on homogenization method. Composite Struct, 2015, 131: 160–170
8 Bai L, Gong C, Chen X, et al. Mechanical properties and energy absorption capabilities of functionally graded lattice structures: Experiments and simulations. Int J Mech Sci, 2020, 182: 105735
9 Niu Y, Yao M H, Zhang W. Nonlinear transient responses of rotating twisted FGM cylindrical panels. Sci China Tech Sci, 2021, 64: 317–330
10 Novak N, Al-Ketan O, Krstulović-Opara L, et al. Quasi-static and dynamic compressive behaviour of sheet TPMS cellular structures. Composite Struct, 2021, 266: 113801
11 Li D, Deng Z, Chen G. Free vibration of functionally graded sandwich plates in thermal environments. Int J Mech Sys Dyn, 2023, 3: 39–47
12 Zhao W, Zhu J, Liu L, et al. A bio-inspired 3D metamaterials with chirality and anti-chirality topology fabricated by 4D printing. Int J Smart Nano Mater, 2023, 14: 1–20
13 Lv C, Qi Y H, Hu R F, et al. Robust, healable and hydrophobically recoverable polydimethylsiloxane based supramolecular material with dual-activate hard segment. Sci China Tech Sci, 2021, 64: 423–432

14 Qi Y H, Zheng J P. An Azo-PDMS-based wearable UV sensor with the optimized photo response mode for dual sensing and synchronous detection. Sci China Tech Sci, 2022, 65: 179–190
15 Kuang X, Wu J, Chen K, et al. Grayscale digital light processing 3D printing for highly functionally graded materials. Sci Adv, 2019, 5: eaav5790
16 Montgomery S M, Hilborn H, Hamel C M, et al. The 3D printing and modeling of functionally graded Kelvin foams for controlling crushing performance. Extreme Mech Lett, 2021, 46: 101323
17 Al-Saedi D S J, Masood S H, Faizan-Ur-Rab M, et al. Mechanical properties and energy absorption capability of functionally graded F2BCC lattice fabricated by SLM. Mater Des, 2018, 144: 32–44
18 Zhang Z, Lei H, Xu M, et al. Out-of-plane compressive performance and energy absorption of multi-layer graded sinusoidal corrugated sandwich panels. Mater Des, 2019, 178: 107858
19 Kholkhoev B C, Bardakova K N, Epifanov E O, et al. A photosensitive composition based on an aromatic polyamide for LCD 4D printing of shape memory mechanically robust materials. Chem Eng J, 2023, 454: 140423
20 Yousuf M H, Abuzaid W, Alkhader M. 4D printed auxetic structures with tunable mechanical properties. Add Manuf, 2020, 35: 101364
21 Ma S Q, Zhang Y P, Wang M, et al. Recent progress in 4D printing of stimuli-responsive polymeric materials. Sci China Tech Sci, 2020, 63: 532–544
22 Spiegel C A, Hackner M, Bothe V P, et al. 4D printing of shape memory polymers: From macro to micro. Adv Funct Mater, 2022, 32: 2110580
23 Lin C, Zhang L J, Liu Y J, et al. 4D printing of personalized shape memory polymer vascular stents with negative Poisson's ratio structure: A preliminary study. Sci China Tech Sci, 2020, 63: 578–588
24 Cecchini L, Mariani S, Ronzan M, et al. 4D printing of humidity-driven seed inspired soft robots. Adv Sci, 2023, 10: e2205146
25 Bodaghi M, Serjouei A, Zolfagharian A, et al. Reversible energy absorbing meta-sandwiches by FDM 4D printing. Int J Mech Sci, 2020, 173: 105451
26 Namvar N, Zolfagharian A, Vakili-Tahami F, et al. Reversible energy absorption of elasto-plastic auxetic, hexagonal, and AuxHex structures fabricated by FDM 4D printing. Smart Mater Struct, 2022, 31: 055021
27 Liu K, Han L, Hu W, et al. 4D printed zero Poisson's ratio metamaterial with switching function of mechanical and vibration isolation performance. Mater Des, 2020, 196: 109153
28 Wang J X, Liu X, Yang Q S, et al. A novel programmable composite metamaterial with tunable Poisson's ratio and bandgap based on multi-stable switching. Compos Sci Tech, 2022, 219: 109245
29 Zeng C, Liu L, Bian W, et al. Compression behavior and energy absorption of 3D printed continuous fiber reinforced composite honeycomb structures with shape memory effects. Add Manuf, 2021, 38: 101842
30 Zeng C, Liu L, Bian W, et al. Bending performance and failure behavior of 3D printed continuous fiber reinforced composite corrugated sandwich structures with shape memory capability. Composite Struct, 2021, 262: 113626
31 Zeng C, Liu L, Bian W, et al. Temperature-dependent mechanical response of 4D printed composite lattice structures reinforced by continuous fiber. Composite Struct, 2022, 280: 114952
32 Yang X, Sun Y, Yang J, et al. Out-of-plane crashworthiness analysis of bio-inspired aluminum honeycomb patterned with horseshoe mesostructure. Thin-Walled Struct, 2018, 125: 1–11
33 Zhang W, Zhang F, Lan X, et al. Shape memory behavior and recovery force of 4D printed textile functional composites. Compos Sci Tech, 2018, 160: 224–230
34 Yazdani Sarvestani H, Akbarzadeh A H, Mirbolghasemi A, et al. 3D printed meta-sandwich structures: Failure mechanism, energy absorption and multi-hit capability. Mater Des, 2018, 160: 179–193
35 Zhang J, Liu Y, Babamiri B B, et al. Enhancing specific energy absorption of additively manufactured titanium lattice structures through simultaneous manipulation of architecture and constituent material. Add Manuf, 2022, 55: 102887
36 Habib F N, Iovenitti P, Masood S H, et al. In-plane energy absorption evaluation of 3D printed polymeric honeycombs. Virtual Phys Prototyping, 2017, 12: 117–131
37 Liu T, Liu L, Zeng C, et al. 4D printed anisotropic structures with tailored mechanical behaviors and shape memory effects. Compos Sci Tech, 2020, 186: 107935